Werk

Jahr: 1982
Kollektion: fid.geo
Signatur: 8 Z NAT 2148:51
Digitalisiert: Niedersächsische Staats- und Universitätsbibliothek Göttingen
Werk Id: PPN1015067948_0051
PURL: http://resolver.sub.uni-goettingen.de/purl?PPN1015067948_0051

LOG Id: LOG_0028
LOG Titel: Observation of guided ULF-waves correlated with auroral particle precipitation theoretically explained by negative Landau damping
LOG Typ: article

Übergeordnetes Werk

Werk Id: PPN1015067948
PURL: http://resolver.sub.uni-goettingen.de/purl?PPN1015067948
OPAC: http://opac.sub.uni-goettingen.de/DB=1/PPN?PPN=1015067948

Contact

Niedersächsische Staats- und Universitätsbibliothek Göttingen
Georg-August-Universität Göttingen
Platz der Göttinger Sieben 1
37073 Göttingen
Germany
Email: gdz@sub.uni-goettingen.de

J Geophys (1982) 51: 119–128

Journal of Geophysics

Observation of Guided ULF-Waves Correlated with Auroral Particle Precipitation Theoretically Explained by Negative Landau Damping

N. Klöcker

Institut für Geophysik und Meteorologie der Technischen Universität Braunschweig, Mendelssohnstraße 3, D-3300 Braunschweig, Federal Republic of Germany

Abstract. Measurements of magnetic and electric field variations in the frequency range 0.3–3 Hz were made on a payload flown as part of the IMS sounding rocket campaign "Substormphenomena". The downward directed Poynting flux of the waves had nearly the same magnitude as the energy flux of the simultaneously observed precipitating electrons. Both phenomena were spatially confined to relatively thin layers. Model computations based on quasi-linear theory taking into account the modification of the electron beam due to the energy transfer exhibit a reasonable agreement with the observed characteristics of the precipitating electron beam, such as speed and temperature, as well as the frequency range and amplitudes of the waves. They support the assumption that the waves were amplified by resonant interaction with the electron beam.

Key words: ULF-waves – Particle precipitation – Wave-particle interaction – Cerencov instability

Introduction

Observations of magnetic field fluctuations with amplitudes of more than 100 nT in the ULF regime obtained by means of a rocket-borne magnetometer were first published by Klöcker and Theile (1979). During the same flight of payload F3A as part of the German IMS sounding rocket campaign "Substormphenomena" magnetic ULF-waves were also observed at an earlier time. Simultaneous measurements of the electric field variations and spectra of precipitating particles provide a data set of reasonable completeness. They allow a comparison with results of model computations of wave-particle interaction in the magnetosphere.

Large amplitude fluctuations with periods 0.2–4 s were detected in the electric field on different rocket flights together with an increase in the precipitating electron flux (Mozer and Fahleson, 1970; Kintner and Cahill, 1978; Petelski et al., 1978). The oscillations were usually confined to regions of small spatial extent. Kintner and Cahill as well as Petelski et al. identified them as magneto-hydrodynamic waves propagating along the geomagnetic field.

In the equatorial plane near the geostationary orbit the ULF-waves are a more or less common phenomenon. Perraut et al. (1978) and the S-300 Experimentors (1979) describe frequently occuring magnetic field variations with amplitudes of 0.3–1 nT with long duration. On the ground Pi/Pc1 pulsations are observed in conjunction with magnetospheric substorms (Kangas et al., 1979).

In this paper an attempt is made to match the observed parameters with model calculations. These are based on the quasi linear theory and on the assumption of resonant interaction between precipitating electrons and Alfvén waves within a thin field-aligned sheet.

Observations

A description of the three-component fluxgate magnetometer was published by Klöcker and Theile (1979). The instrumentation of the payload as well as the geophysical conditions during launch on October 13, 1977, at 21:26:00 UT are described in detail by Wilhelm et al. (1981). The two successive ULF events under discussion here occurred at about 21:30 UT when the payload reached the northern boundary of the auroral activity at a height of about 400 km. They coincide with observations of field-aligned current sheets as indicated in Figs. 1 and 2. The lower curves show the three magnetic field components in a coordinate system which is fixed to the earth's magnetic field, i.e. B_z is parallel to the undisturbed field $\mathbf{B}^E$, B_x points to magnetic north and B_y completes the right-handed coordinate system pointing towards magnetic east. The field data were transferred from the gyrating payload system into this coordinate system by unitary transformations after the misaligned sensor system had been corrected into an orthogonal, normalized, and spin oriented coordinate system. This operation was complicated by the rather unstable payload rotation. Because of energy dissipation in the long flexible booms, the nutation angle increased so rapidly that an activation of the attitude control system was necessary about every 60 s. The data gap between 216 s–224 s after launch is due to this. The coherently occuring transient oscillations in B_x and B_y with the nutation frequency of 0.3 Hz are also a consequence of the high variability of the attitude parameters. As the fit of these parameters by time functions of limited order cannot be an ideal one within a relative error of 1×10^{-4}, the small deviations produce apparent wave fields. To eliminate a trend in B_z a reference field for B^E was sub-

0340-062X/82/0051/0119/$02.00

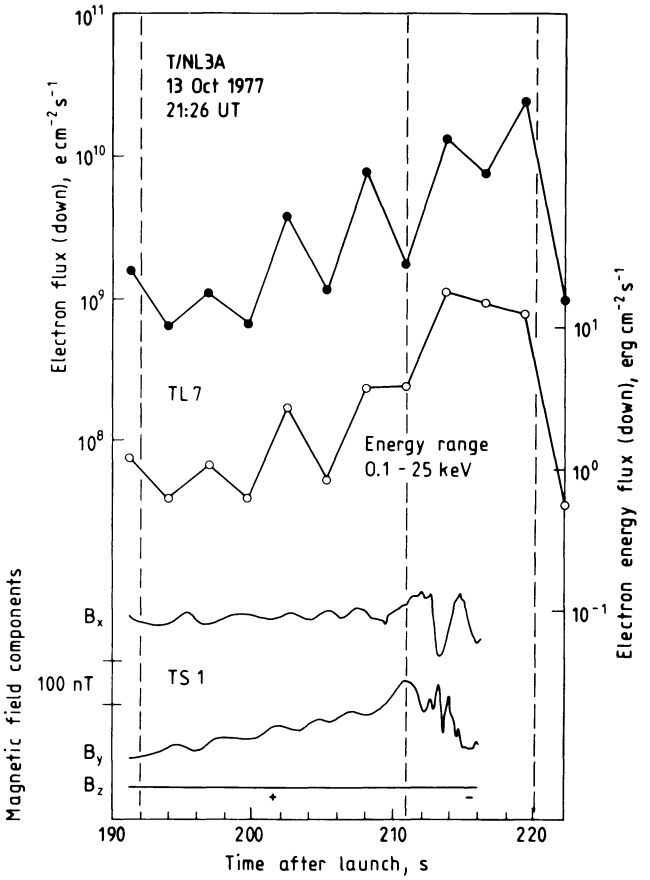

Fig. 1. Comparison between electron flux data and magnetic field observations made aboard payload T/NL 3A during the time interval 192–220 s elapsed time. The apparent, smooth wave forms occuring coherently in the B_x and B_y components result from residual nutation contributions to the total magnetic field. The coordinate system is fixed to the earth's magnetic field. Regions marked + and − are characterized by downward- and upward-directed currents, respectively (from Wilhelm et al., 1981)

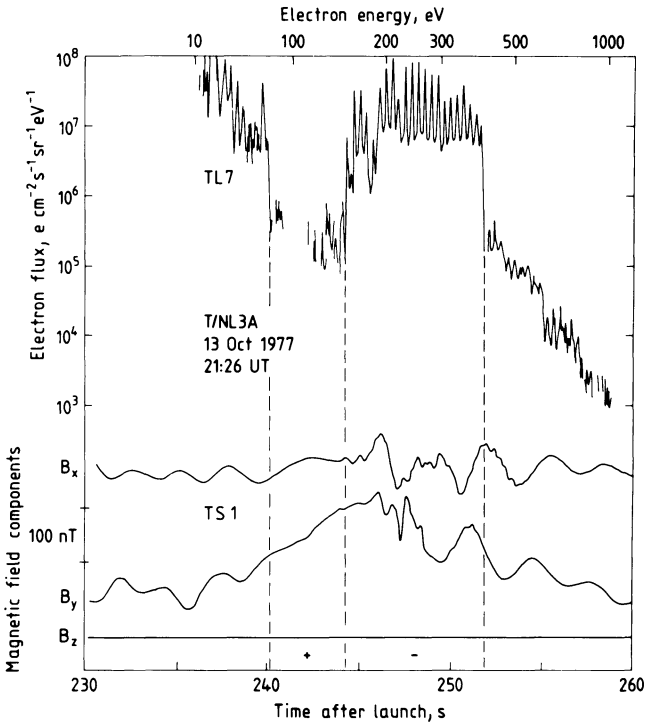

Fig. 2. High time resolution electron flux measurements compared to magnetic field observations as in Fig. 1 for 230–260 s elapsed time (from Wilhelm et al., 1981)

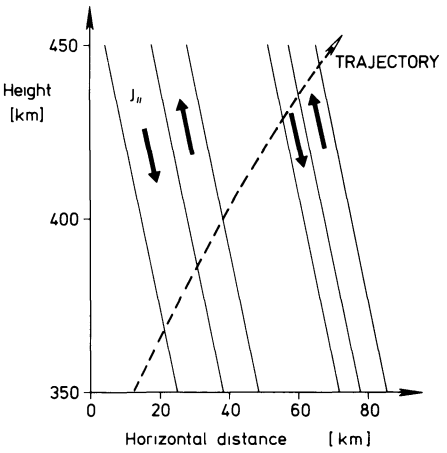

Fig. 3. Schematic picture of the flight path of the payload relative to the current sheets. The payload had a horizontal velocity of 860 m/s and a vertical velocity ranging from 1,800 m/s at 350 km height down to 1,200 m/s at 450 km. The horizontal direction of motion was 20° W of geographic north. The beginning of the horizontal scale is arbitrarily chosen

stracted from the transformed z-component. Figure 3 shows the flight pass of the payload relative to the field-aligned current sheets.

Both events are characterized by very similar signatures in the B_y-component, i.e. a constant increase and subsequent decrease, indicating oppositely directed current sheets. This interpretation is supported by the low energy electron measurements also presented in Figs. 1 and 2. (For a more detailed description see Wilhelm et al., 1981.) The fluctuations we are concerned with appeared in both cases confined to the northern upward-directed current sheets. They are shown again in Figs. 4 and 5 with an extended time scale and suppressed long period variations. The high-pass filter used has a cut-off frequency of 0.25 Hz.

The wave vector is purely transverse to the undisturbed magnetic field, since B_z exhibits no variations. Therefore it seems appropriate to separate the wave vector into its circular-polarized parts and compare the subsequent Fourier-analyzed magnetic data with the electric field data treated in the same manner in order to identify the observed wave mode. Figures 6 and 7 show the frequency spectra of **E** and **B** for the two events. In both figures the righthand and lefthand polarized parts are drawn separately. The close agreement of the spectra for at least the first event justifies the interpretation of our observations in terms of Alfvén waves. They were more or less linearly polarized. This assumption is confirmed if we compare the wave phase velocities derived from the observed wave fields with the estimated Alfvén velocity $v_A = B^E/\sqrt{\mu_0 nm}$. The amplitude ratio E_{oi}/B_{oi} $(i = rh, lh)$ lies between 1,000 and 1,500 km/s. With the plasma

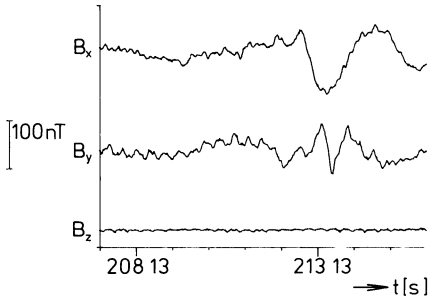

Fig. 4. High-pass filtered magnetic field data for the first event. The boundary between the antiparallel current sheets was crossed at 211 s after launch

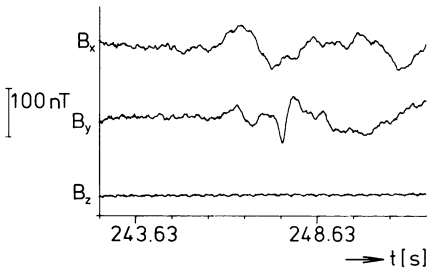

Fig. 5. High-pass filtered magnetic field data of the second event. At 244 s the payload entered the upward directed current sheet

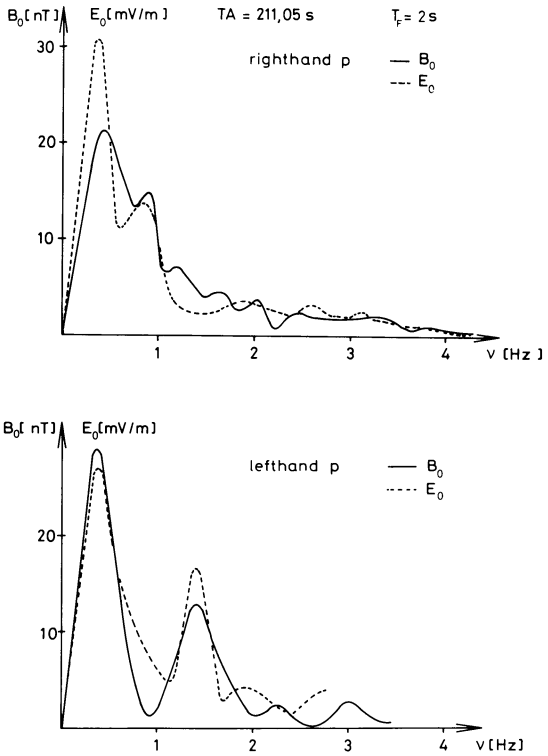

Fig. 6. Comparison of the frequency spectra of the electric and magnetic field vectors during the first event. The right-hand (*upper part*) and lefthand (*lower part*) polarizations are drawn separately. B_0 and E_0 indicate the amplitudes of the waves. *TA* is the time after launch at which the time window is opened, it's length being 2 $T_F = 4$ s

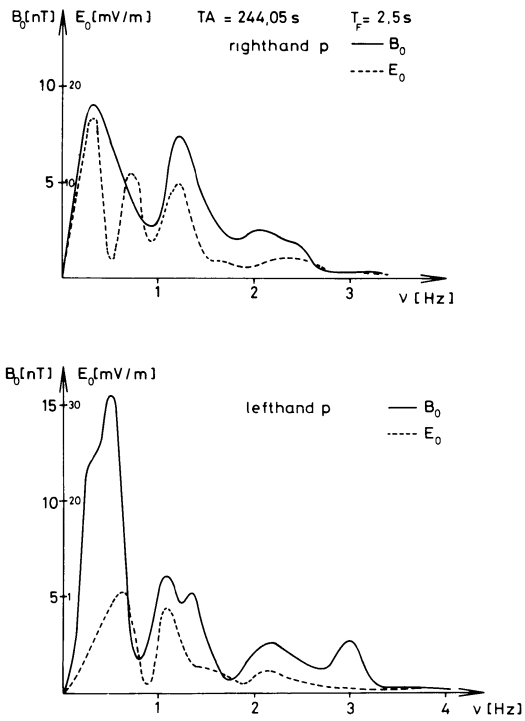

Fig. 7. As Fig. 5 but for the second event

density measured on board $n = (1.5 \pm 0.1)\ 10^{10}\,\mathrm{m}^{-3}$ we get $v_A \approx 2{,}000$ km/s if O^+-ions dominate and $v_A \approx 1{,}500$ km/s for the case that the ion population consists predominantly of NO^+-ions.

Direction and amplitude of the wave field vectors are plotted in Fig. 8 versus time after launch. During time intervals of about 2 s the phase difference between **E** and **B** remains at nearly 90°, yielding a Poynting flux $\mathbf{S} = \mathbf{E} \times \mathbf{B}/\mu_0$ in the direction of the precipitating electrons. The energy fluxes carried by the electrons and the Alfvén waves are of comparable magnitude. In the first event they amount to $15 \cdot 10^{-3}\,\mathrm{J/m^2\,s}$ and $3 \cdot 10^{-3}\,\mathrm{J/m^2\,s}$, respectively.

Consideration of the observed energy spectra of the precipitating electrons completes this unique data set. Figure 9 shows a sequence of energy spectra during the first event. Outside the upward-directed current sheet the spectrum can be approximated by a single power law $F(W) \sim W^{-\gamma}$, with the exponent $\gamma = 2.3$ (Wilhelm et al., 1981). During the period with increased flux the spectrum changes considerably. Superimposed on the power law spectrum is an electron beam with a mean velocity $v_{\parallel} = 2.5 \cdot 10^4$ km/s corresponding to $W_{\parallel} = 1.8$ keV and a thermal velocity $v_{the} = 3.5 \cdot 10^3$ km/s corresponding to 35 eV. Taking into account the measured pitch angle distribution the beam distribution function can be represented by an anisotropic Maxwellian function:

$$f_e'(\mathbf{u}) = \frac{n_e}{(2\pi)^{3/2}\, v_{the\perp}^2\, v_{the\parallel}}\, e^{-\frac{u_\perp^2}{2 v_{the\perp}^2} - \frac{(u_\parallel - v_\parallel)^2}{2 v_{the\parallel}^2}} \qquad (1)$$

n_e is of the order of $1\ 10^6\,\mathrm{m}^{-3}$. The perpendicular thermal velocity $v_{the\perp}$ is about twice as large as $v_{the\parallel}$.

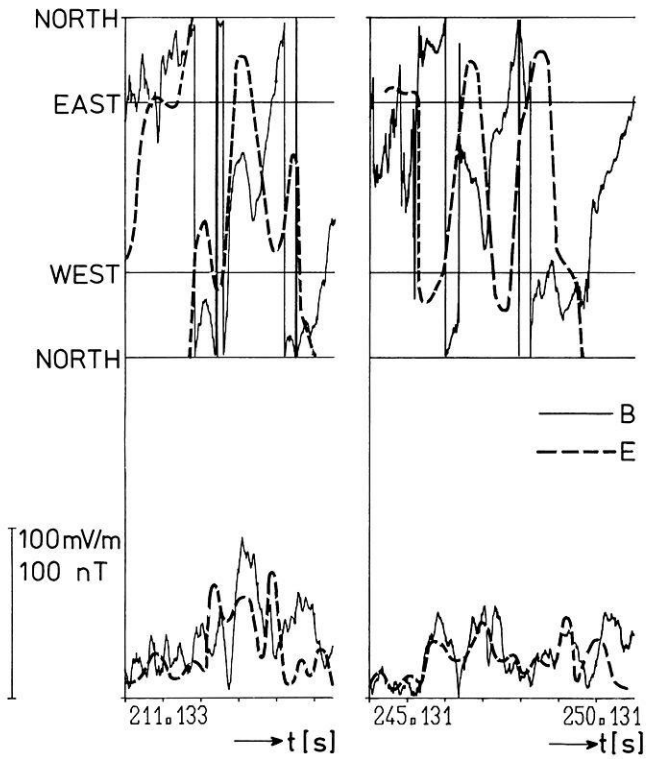

Fig. 8. Comparison of the direction (*upper part*) and amplitude (*lower part*) of the wave vectors **E** and **B** for the two events. During the time intervals 211.5 s–213.5 s after launch and from $t=245.2$ s–247.2 s the phase difference between E and B approaches about 90°. $\mathbf{E}\times\mathbf{B}$ points downward

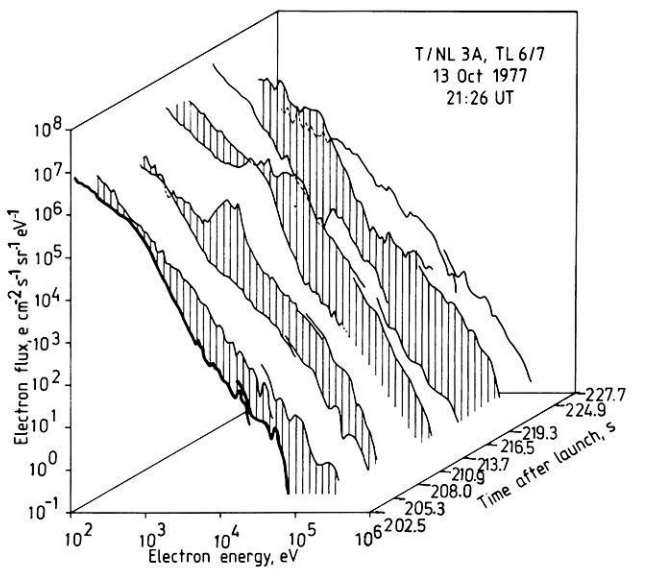

Fig. 9. Electron energy spectra as measured during the first of the events described. The observations were made by two instruments in different energy ranges with some overlap near 25 keV (from Wilhelm et al., 1981)

The Cerencov Instability

The remarkable spatial correlation between the electron beam and the ULF-waves in the two events, their extreme similarity and their small spatial extent, of the order of a few km, suggest an interaction mechanism between the beam and the waves such as was theoretically investigated by Fejer and Kan (1969). Starting from the examination of the guided propagation of Alfvén waves along the external magnetic field (Fejer and Lee, 1967) they derived the growth rate of Alfvén waves by 'negative Landau damping'. The essential attribute of guided Alfvén waves in a cold plasma is their small spatial extent perpendicular to $\mathbf{B}^E$, i.e. the wave number $k_\perp$ exceeds $k_\parallel$ considerably. As a consequence the component of the electric wave field in the direction of $\mathbf{B}^E$ is not neglegible. If the amplitude profile of the spatially confined waves perpendicular to the propagation direction is approximated by a Gaussian function with d as the $1/e$-width in x, assuming no y-dependency, then according to Fejer and Lee (1967) the width d is bounded by the inequality

$$4\frac{c}{\omega_{pe}} \ll d \ll 4\frac{v_A}{\omega}. \tag{2}$$

c is the speed of light, ω the wave frequency, and ω_{pe} is the electron plasma frequency. Under these conditions most of the power is radiated into a beam along the homogeneous ambient magnetic field, whose angular width is considerably less than 0.1°. The in situ measurements provide an upper and lower limit of 5,000 km and 250 m, respectively. The observed values for $d\approx 3$ km in the first and about 5 km in the second event are at least one order of magnitude inside the limits and therefore satisfy the inequality quite well.

In the presence of guided Alfvén waves with phase velocities near the bulk velocity of the electron beam (1) this distribution is unstable (Fejer and Kan, 1969). The resonant growth rate k_{zI}, i.e. the imaginary part of the complex wave number $k_z=k_{zR}+ik_{zI}$ parallel to $\mathbf{B}^E$, is given by Fejer and Kan as

$$k_{zI}=\sqrt{\frac{\pi}{8}}\frac{n'_e}{n_e}\frac{k_x^2}{k_{zR}^4}\frac{\omega^4}{\omega_{pe}^2}\frac{S}{v'^3_{the}}(\omega-k_{zR}v_z)\,e^{-z_{eo}^2} \tag{3}$$

where n_e, n'_e are the electron densities of the ambient plasma and the beam, respectively (the primed values denote the beam).

$$\begin{aligned} S &\equiv \sum_\alpha \frac{\omega_{p\alpha}^2}{\omega_{c\alpha}^2-\omega^2} \\ \omega_{p\alpha}^2 &= \frac{q_\alpha^2 n_\alpha}{\varepsilon_0 m_\alpha} \\ \omega_{c\alpha} &= \frac{q_\alpha B^E}{m_\alpha} \\ z_{eo} &= \frac{\omega-k_{zR}v_z}{\sqrt{2}k_{zR}v'_{the\parallel}} \end{aligned} \tag{4}$$

where q_α is the elementary charge of the ion component α and m_α its mass. Under the condition that $\omega_{p\alpha}\gg\omega_{c\alpha}$, $\omega_{p\alpha}\gg\omega$, and $m_\alpha\gg m_e$, S is one of the diagonal elements of the dielectric tensor of a cold plasma.

The sign of k_{zI} determines the direction of the energy flow. If $v_z>v_{ph}$, the phase velocity of the wave, k_{zI} is negative, i.e. instability occurs. The exponent of (3) together with the factor n'_e/v'^3_{the} indicate the number of

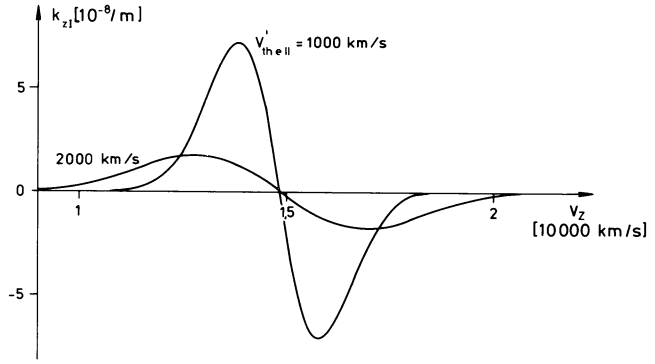

Fig. 10. The growth rate k_{zI} as a function of the bulk velocity v_z of the electron beam. The assumed parameters may be typical for a magnetospheric plasma $3R_E$ from the earth's centre

beam particles which are in resonance with the wave. Therefore the growth rate increases with decreasing beam temperature as is shown in Fig. 10. k_{zI} is calculated as a function of v_z, the mean beam velocity, in a plasma which may be typical for the magnetosphere at a distance of about $3R_e$ (earth radii) from the earth's center, i.e. $B^E = 2{,}000\,\mathrm{nT}$, $n_e = 10^7\,\mathrm{m}^{-3}$, $n'_e/n_e \approx 10^{-2}$. These conditions provide an Alfvén velocity $v_A \approx 15{,}000\,\mathrm{km/s}$ and a parallel wave number $k_{zR} \approx 7 \cdot 10^{-7}\,\mathrm{m}^{-1}$ if $\omega = 10\,\mathrm{rad/s}$ is assumed. k_x may be $10^{-4}\,\mathrm{m}^{-1}$ which is the upper limit for a wave packet with a perpendicular extent of 40 km. With an appropriate k_x satisfying (2) and $\omega \ll \omega_{c\alpha}$ the growth rate is a linear function of ω. But only for frequencies less than the ion cyclotron frequency can this wave mode propagate. In the described plasma $\omega_{ci} \approx 200\,\mathrm{rad/s}$ only under the condition that protons are present. This value is lowered considerably if e.g. He^+-ions contribute to the ion population.

If we consider the resonant interaction between the electron beam and the waves as a realistic mechanism for the amplification of the waves and further note the large Poynting flux in relation to the energy flux of the beam the question arises how the beam itself is affected by the interaction. An answer can be given in terms of quasi-linear kinetic theory. The following considerations are based on a publication of Kennel and Engelmann (1966). They derived the quasi-linear velocity space diffusion equation for waves of any oscillation branch propagating at an arbitrary angle to a uniform external magnetic field. The space- and time-averaged distribution function of the beam is assumed to change slowly compared to a gyroperiod and to the characteristic times of the wave motion. Kennel and Engelmann's theory is restricted to a collisionless, infinite, and spatially uniform plasma immersed in a static magnetic field with no curvature, which can only be a very rough model of the near earth magnetosphere.

The electric field vector of an Alfvén wave propagating within a thin layer has the following components (Fejer and Lee, 1967):

$$E_r = \tfrac{1}{2}\left(1 + \frac{\omega_{pe}^2}{c^2}\frac{D}{k_x^2(S-P)}\right)E_x$$

$$E_l = \tfrac{1}{2}\left(1 - \frac{\omega_{pe}^2}{c^2}\frac{D}{k_x^2(S-P)}\right)E_x \tag{5}$$

$$E_z = \frac{k_x k_{zR}}{k_x^2 + \dfrac{\omega_{pe}^2}{c^2}}E_x$$

where E_r and E_l are the righthand and lefthand polarized parts of the field in a plane perpendicular to the external magnetic field. They are defined on the basis $\mathbf{e}_r \equiv \mathbf{e}_x + i\,\mathbf{e}_y$ and $\mathbf{e}_l \equiv \mathbf{e}_x - i\,\mathbf{e}_y$, respectively.

D, S, and P are the elements of the dielectric tensor of a cold plasma. S is already defined in (4). The other expressions are:

$$D \equiv -\sum_\alpha \frac{\omega_{p\alpha}^2 \omega}{\omega_{c\alpha}(\omega_{c\alpha}^2 - \omega^2)}$$
$$P \equiv -\frac{\omega_{pe}^2}{\omega^2}. \tag{4a}$$

The local dependency of the electric wave field which is confined to a comparably narrow tube of force can be written in the form:

$$E_x(x, z, t) = E_0\, e^{-\frac{4x^2}{d^2}}\, e^{i(k'_z z - \omega' t)} \tag{6}$$

whose Fourier transform in a space-time element V with the lengths L_x, L_y, and T is

$$\begin{aligned} E_x(k_x, k_y, \omega, z) &= \int_V E_x(x, z, t)\, e^{-i(k_x x + k_y y - \omega t)}\, dx\, dy\, dt \\ &= E_0 \frac{\sqrt{\pi}}{2} d\, e^{-\frac{d^2 k_x^2}{16}}\, e^{ik'_z z} \\ &\quad \cdot 2\frac{\sin\frac{L_y}{2}k_y}{k_y} \cdot 2\frac{\sin\frac{T}{2}(\omega - \omega')}{\omega - \omega'}. \end{aligned} \tag{7}$$

Substituting these quantities into Kennel and Engelmann's Equation (2.24) in a convenient way, as outlined in the Appendix, we obtain the spatial derivative in the direction of z of the beam distribution function

$$\frac{\partial f'_{oe}}{\partial z} \approx \frac{\sqrt{2\pi}}{d^2}\frac{E_0^2}{\mu_0}\frac{\omega^2}{n_e m_e}\frac{S}{\omega_{pe}^2}\frac{1}{u_z}\frac{\partial}{\partial u_z}\frac{-k_{zI}u_z}{|\omega - k_z u_z|^2}\frac{\partial f'_{oe}}{\partial u_z}. \tag{8}$$

Together with the linear approximation

$$\frac{\partial E_0^2}{\partial z} = -2k_{zI}E_0^2 \tag{9}$$

and the expression (3) for the growth rate we have a complete set of coupled equations to estimate the energy transfer between the particle beam and the waves and their mutual dependency along a magnetic field line. The parameters of the wave propagation are still governed by the cold stationary background plasma.

For a complete computation of the instability in terms of (3), (8), and (9) we must know the frequency spectrum of the waves and the energy spectrum of the

beam at the point $z=0$ where the beam starts. This information is not available. In case of the wave spectrum the payload could only observe waves with periods shorter than the transit time through the upward-directed current sheet. In addition we observed the results of the interaction and not the original conditions. Therefore it seems appropriate to assume the beam distribution function as Maxwellian along the whole path covered and to examine the variation of the characterizing parameters which are v_z and $v_{the\parallel}$. This is done in determining the energy transfer, i.e. the divergence of the energy flux of the electrons or the waves.

Let $\mathbf{v}\cdot W_e$ be the kinetic energy flux density of the electron beam and $\mathbf{S}$ the Poynting flux. Then the energy balance condition has the form

$$\nabla\cdot(\mathbf{v}\cdot W_e)=-\nabla\cdot\mathbf{S}$$

with

$$\mathbf{v}\cdot W_e=\tfrac{1}{2}m_e\int\mathbf{u}\,u^2 f'_{oe}\,d^3u, \tag{10}$$

$$\mathbf{S}=\lim_{V\to\infty}\frac{1}{(2\pi)^3 V}\int_V\frac{1}{\mu_0}\mathbf{E}^*\times\mathbf{B}\,dk_x\,dk_y\,d\omega. \tag{11}$$

Since $\mathbf{v}=(0,0,v_z)$ we obtain for the beam:

$$\frac{\partial}{\partial z}(v_z W_e)=\pi m_e\int_{-\infty}^{\infty}\int_0^{\infty}u_z u_\perp(u_\perp^2+u_z^2)\frac{\partial f'_{oe}}{\partial z}\,du_\perp\,du_z. \tag{12}$$

This is a sum of two integrals. The first one vanishes, since together with (8) the integrand is a pure derivative with respect to u_z, and the distribution function and all its derivatives tend to zero at infinity. This indicates that the particle motion perpendicular to the ambient magnetic field is not affected by the instability.

For a sufficient small growth rate the factor with k_{zI} in (8) can be replaced by a delta function.

$$\lim_{k_{zI}\to 0}\frac{-u_z k_{zI}}{(\omega-k_{zR}u_z)^2+(u_z k_{zI})^2}=-\pi\,\delta(\omega-k_{zR}u_z)$$
$$=\frac{\pi}{k_{zR}}\,\delta\left(u_z-\frac{\omega}{k_{zR}}\right).$$

This approximation is equivalent to neglecting nonresonant interaction which in first order is a linear function in k_{zI} (Kennel and Engelmann, 1966). The integral (12) finally yields:

$$I=\sqrt{\frac{\pi}{2}}\,m_e\frac{\omega}{k_{zR}^2}\frac{n'_e}{v'^3_{the\parallel}}\left(\frac{\omega}{k_{zR}}-v_z\right)e^{-z_e^2/2} \tag{13}$$

for the energy transfer from the beam to the wave.

The gain of the Poynting flux in case of negative k_{zI} is described by the expression

$$\frac{\partial S_z}{\partial z}=-\lim_{V\to\infty}\frac{2}{v_{ph}(2\pi)^3 V}\int_V k_{zI}\frac{|E|^2}{\mu_0}\,dk_x\,dk_y\,d\omega$$

following from (11) and (9) with the approximation $B_y\approx E_x/v_{ph}$ which implies that nearly all the wave energy is stored in the magnetic field. Except for the sign the result coincides with (13). The integration follows the same way as is outlined in the Appendix. The complete expression has the form:

$$\frac{\partial S_z}{\partial z}=-\pi\frac{E_0^2}{\mu_0}\frac{n'_e}{n_e}\frac{\omega^3}{d^2k_{zR}^2}\frac{S}{\omega_{pe}^2}\frac{1}{v'^3_{the\parallel}}\cdot\left(\frac{\omega}{k_{zR}}-v_z\right)e^{-z_e^2/2}. \tag{14}$$

Now we can return to our original aim of examining the rate of change of v_z and $v_{the\parallel}$ due to the instability. For this purpose we separate the kinetic energy of the beam W_e into its energy of the center of mass motion W_{e1} and its inner energy W_{e2} with

$$W_e=W_{e1}+W_{e2}$$
$$=\tfrac{1}{2}n'_e m_e(2v'^2_{the\perp}+v'^2_{the\parallel}+v_z^2) \tag{15}$$

and $W_{e2}=\frac{1}{2}m_e\int(\mathbf{u}-\mathbf{v})^2 f'_{oe}\,d^3u$.

The divergence of the flux of the inner energy $\mathbf{v}W_{e2}$ can be derived in the same way as the divergence of the total flux. The relation is

$$\frac{\partial}{\partial z}(v_z W_{e2})=\left(\frac{\omega}{k_{zR}}-v_z\right)\frac{k_{zR}}{\omega}\frac{\partial}{\partial z}(v_z W_e).$$

With this result it follows from (15) that

$$\frac{\partial}{\partial z}(v_z W_{e1})=\frac{k_{zR}}{\omega}v_z\frac{\partial}{\partial z}(v_z W_e)$$
$$=\frac{m_e}{2}\frac{\partial}{\partial z}n'_e v_z^3.$$

With respect to the continuity equation $\nabla\cdot(\mathbf{v}\cdot n'_e)=0$ or

$$\frac{\partial n'_e}{\partial z}=-\frac{n'_e}{v_z}\frac{\partial v_z}{\partial z}$$

we finally obtain the relation

$$\frac{\partial v_z}{\partial z}=-\frac{k_{zR}}{\omega}\frac{1}{n'_e m_e v_z}\frac{\partial S_z}{\partial z}. \tag{16}$$

Since, as has already been shown, the perpendicular velocity component does not change during the instability, it follows from (15) and (16) that

$$\frac{\partial v'_{the\parallel}}{\partial z}=\left(\frac{\omega}{k_{zR}}-v_z\right)\frac{1}{v'_{the\parallel}}\frac{\partial v_z}{\partial z}. \tag{17}$$

Model Calculations

In contrast to the conditions limiting the theoretical considerations, the near-earth magnetosphere is much more complex and, more importantly, inhomogeneous. An application of the theory outlined is therefore only valid in narrow regions in which the magnetospheric parameters can be approximated by constant values. On the other hand the extent of these regions should be at least of the order of the wave length. With this contradiction in mind we must realize that the theoretical results can only give a rough picture of the actual processes. Nevertheless this picture shows essential characteristics which are in agreement with the observations.

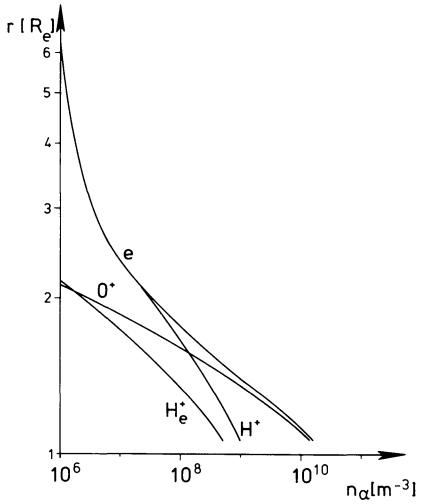

Fig. 11. Height distribution of the ionic constituents of the model magnetosphere

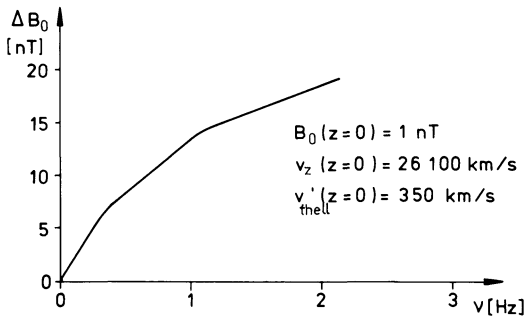

Fig. 12. The gain of the wave amplitude ΔB_0 due to the wave-particle interaction along a flux tube with $L=7$ at a hight of 400 km as a function of the wave frequency

The calculations are based on a dipolar magnetospheric model whose ionic constituents are H^+, He^+, and O^+. Their assumed height distribution is shown in Fig. 11. Since we are interested in the variation of the bulk velocity and the thermal velocity parallel to the external magnetic field caused by the instability the effect of conservation of the first adiabatic invariant must be taken into account. In a converging magnetic field kinetic energy is transferred from the parallel motion into the perpendicular velocity component. The mapping of an anisotropic Maxwellian distribution along field lines was studied by Chiu and Schulz (1978). Taking their equations the estimated variation of the bulk velocity between the equator and the upper ionosphere along a field line with an equatorial distance of $7R_e$ is relatively small. v_z is reduced from 2.0×10^7 m/s to 1.9×10^7 m/s. In contrast, $v_{the\perp}$ changes by about a factor of 10.

The following figures illustrate the dependency of the coupling between particles and field on various parameters, such as the frequency of the wave (Fig. 12), the width of the beam parallel to the ambient magnetic field (Fig. 13), and the bulk velocity of the beam (Fig. 14). If the interaction were to take place in a homogeneously magnetized plasma, Equation (14)

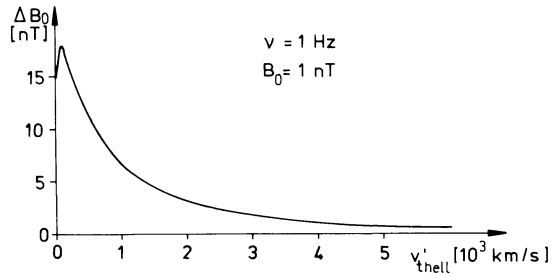

Fig. 13. ΔB_0 as in Fig. 12 at 400 km hight as a function of the parallel thermal velocity of the beam

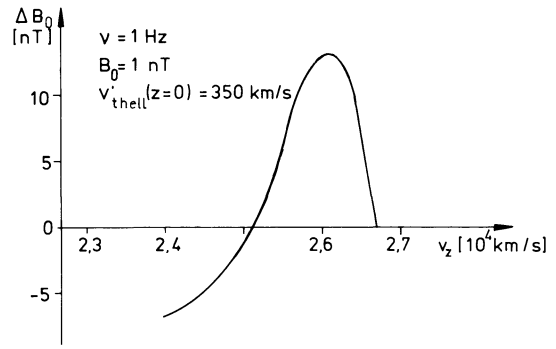

Fig. 14. ΔB_0 as in Fig. 12 as a function of the bulk velocity of the electron beam

would demand a linear increase of the Poynting flux with frequency or an increase of the wave amplitude with $\sqrt{\nu}$. The curve in Fig. 12 shows this behaviour, where ΔB_0 represents the gain of the wave amplitude due to the interaction, computed at a height of 400 km. ν is limited to lower values than the ion cyclotron frequencies.

The influence of the model magnetosphere on the interaction along a flux tube is more evident in the dependency of ΔB_0 on $v'_{the\,\|}$, as shown in Fig. 13. Since the resonant velocity, i.e. the Alfvén velocity, passes through a maximum along a magnetic field line, particles and fields can only exchange energy along a finite length of path. But this length is a function of the parallel beam temperature, because a beam with a broad thermal velocity distribution covers a larger velocity range. Therefore ΔB_0 does not behave as $v'^{-1.5}_{the\,\|}$, rather it begins to decrease as $v^{-0.5}_{the}$ and changes over to $v^{-1.3}_{the}$.

Figure 14 shows ΔB_0, always at the height of 400 km, as a function of the bulk velocity v_z of the beam. For v_z near to and less than the maximal wave phase velocity the direction of the energy transfer turns over. In this case the Alfvén wave is Landau damped. This might be the reason for the fact that no waves were observed outside of the electron beams. As is shown in the last figure (Fig. 15), the amplitude of a guided wave would rise to about 20 nT from a value of 1 nT near the equatorial plane due to energy flux conservation alone. Since waves of this type and magnitude have often been observed on GEOS II their rare occurrence at lower heights can be explained by Landau damping.

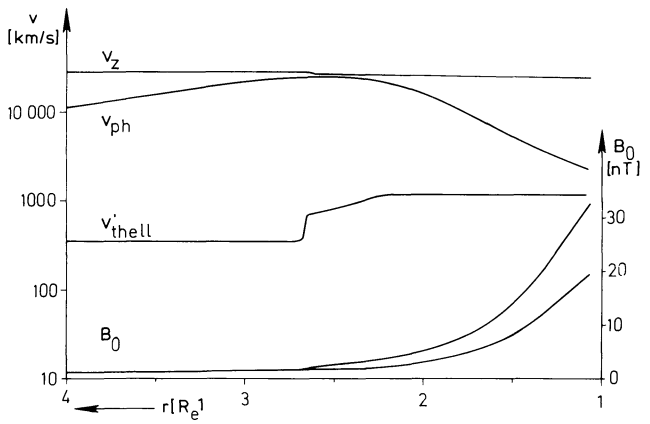

Fig. 15. The evolution of the wave-particle interaction along a flux tube with $L=7$ in the model magnetosphere. The characteristic parameters are the bulk velocity v_z, the wave phase velocity v_{ph}, the parallel thermal velocity of the electron beam $v'_{the\,\|}$, and the amplitude of the wave field B_0. $\nu=1$ Hz. The lower line of B_0 shows the increase of the amplitude due only to energy flux conservation

Figure 15 also provides information about the location in the model magnetosphere where the interaction takes place. This is between 2 and $3R_e$, where v_{ph} has its maximum, and the complex wave number k_{zI} reaches a value which is a factor of 10 or less smaller than k_{zR}.

Discussion and Conclusions

The set of observations presented here is the first reasonably complete description of electromagnetic ULF-waves in connection with auroral electron precipitation. During two successive events we observed, at the height of the ionospheric F-region, electromagnetic waves confined to thin field-aligned current sheets. We interpret these fluctuations in terms of Alfvén waves, since their phase velocities were of the same order of magnitude as the Alfvén velocity estimated theoretically. Secondly, only Alfvén waves can show such large wave numbers perpendicular to the ambient magnetic field.

The last argument, involving the condition $k_{\|} \ll k_{\perp}$ which is important for the whole theory, is based on the assumption that the payload crossed a more or less steady structure. This is supported by all-sky camera photographs showing a steady northern boundary of the active arc region during the passage of the payload (Wilhelm et al., 1981). Also the current sheets, observed simultaneously both in **B** and in the electron flux, which exhibit a time scale and signature in the payload system quite distinct from the wave-like fluctuations, make it more likely that we observed guided waves rather than a transient phenomenon.

The observed net energy flux of the waves stands against the possible interpretation as standing waves or field line resonance. The Poynting vector pointed downwards for at least 2 s in each event. The subsequent transition to a more turbulent behaviour at 213.5 s and at 247.2 s, respectively (Fig. 8), is probably due to reflection at the ionospheric E-layer. The spatial separation between the incoming and reflected waves can then be explained by a southward motion of the arc. Since the Alfvén velocity decreases rapidly to a value of below 1,000 km/s with decreasing height, a separation of 2 km at about 300 km above the E-layer corresponds to a southward drift of approximately 1 km/s. This is in agreement with the observations.

An explanation of the waves in terms of the cyclotron instability and pitch angle diffusion near the equator has been excluded for several reasons. This mechanism is often discussed in literature (Engel, 1965; Cornwall, 1966; Kennel and Petschek, 1966; Gendrin, 1968; Coroniti and Kennel, 1970). (A very useful technique to determine the sign of the imaginary part of the wave number is published by Gendrin (1981).) First, an explanation in terms of the cyclotron instability would not answer the question of the correlation with the precipitating electrons. In addition, the observed frequencies are too high for gyroresonance at the equator, especially if not only protons are present. For waves propagating at an angle to the magnetic field, integral multiples of the gyrofrequency can be amplified. But the instability is most effective for $k_{\perp}=0$. Thus we would not expect such a thin spatial confinement of the events.

In agreement with the arguments of Stüdemann and Goertz (1981), who explain observed ULF-waves associated with an energetic proton beam in terms of 'kinetic Alfvén waves' (Hasegawa, 1977), these observations demand a similar interpretation. Such a hypothesis is further supported by the model calculations described above. The results indicate that under special conditions (Fejer and Lee, 1967) the component of the wave electric field, which is parallel to the guiding magnetic field, is strong enough for an appreciable energy exchange between the electron beam and the waves. The observed parameters agree well with the computed results.

Nevertheless one should keep in mind that the boundary conditions of the underlying theory are probably violated by the properties of the model magnetosphere. Plasma and ambient magnetic field are not homogeneous within the characteristic scale length, i.e. the wave length of the Alfvén waves. Due to flux conservation, the change of the wave amplitude is of the same order of magnitude as the change of the wave vector itself, which is not taken into account. Furthermore the complex wave number k_{zI} can grow up to values of the order of the real wave number k_{zR}, which can occur at the beginning of the interaction. So the application of the linear theory might be doubtful. As a consequence these considerations and model computations can give only a rough and tentative picture of the actual physical processes by which free energy is transferred to and exchanged between particles and fields.

The question of the origin of the beam has not been answered. The reverse process of the waves generating the beam can be excluded, because it would require a wave amplitude outside $3R_e$ of about 10 nT, which seems to be unrealistically high. In addition it would require a much longer interaction with slowly increasing Alfvén velocity to accelerate the electrons from about 300 eV, where we find a sufficiently high particle density in the spectrum, up to 1.8 keV. It would also leave open the question of the origin of the waves. But

the model presented provides a boundary condition for possible acceleration mechanisms which are currently discussed. The incoming beam must exist outside the region of maximal Alfvén velocity, i.e. at $r \gtrsim 2.5 R_e$. This condition is not inconsistent with the theory of electrostatic shocks or double layers. The $n=0$ ion cyclotron mode instability is a possible candidate from which oblique shocks evolve (Swift, 1978). They may form where the relative streaming speed between ions and electrons exceeds the threshold for excitation of the $n=0$ ion cyclotron wave. This will occur along the flux tube where the ion density times the flux tube cross section has a minimum. In our model this minimum is located around $r \approx 3 R_e$. Furthermore the small spatial extent of the observed current sheets and the mode of the amplified waves fit well with the theory of V-shocks reviewed by Swift (1978).

Acknowledgements. This article is a short version of the author's thesis. Therefore I wish to thank especially Professor Dr. W. Kertz, Direktor des Instituts für Geophysik und Meteorologie der TU Braunschweig, for many fruitful discussions and steady support of my work. Furthermore I thank Dr. B. Theile, the experiment scientist for the magnetometer work, for his support and also Dr. H. Lühr, who performed the hardware side of the experiment. New ideas developed in discussions with Dr. C.K. Goertz, Max-Planck-Institut für Aeronomie, Lindau. Measurements from additional instruments of the same payload were kindly provided by Dr. R. Grabowsky, Fraunhofer-Institut für Physikalische Weltraumforschung, Freiburg, and Dr. K. Wilhelm, Max-Planck-Institut für Aeronomie, Lindau, who acted as project scientist.

The rocket program "Substormphenomena" was funded by the "Bundesministerium für Forschung und Technologie" and managed by the DFVLR-BPT

Appendix

The diffusion equation of Kennel and Engelmann (1966) reads

$$\frac{\partial f'_{o\alpha}}{\partial z} = \lim_{V\to\infty} \frac{1}{(2\pi)^3 V} \frac{q_\alpha^2}{u_z m_\alpha^2} \sum_{l=-\infty}^{\infty} \int k_\perp \, dk_\perp \, d\psi \, d\omega \left[\left(\hat{G} + \frac{\omega - k_z u_z}{\omega u_\perp} \right)^* \mathscr{E}^*_{l\alpha} + \hat{K}^*_{l\alpha} J_l E^*_z \right] \frac{i}{\omega - k_z u_z - l\omega_{c\alpha}} [\mathscr{E}_{l\alpha} \hat{G} + E_z J_l \hat{K}_{l\alpha}] f'_{o\alpha} \tag{A1}$$

with the following substitutions

$$\hat{G} \equiv \left(1 - \frac{k_z u_z}{\omega}\right) \frac{\partial}{\partial u_\perp} + \frac{k_z u_\perp}{\omega} \frac{\partial}{\partial u_z}$$
$$\hat{K}_{l\alpha} \equiv \frac{\partial}{\partial u_z} + \frac{l\omega_{c\alpha}}{\omega u_\perp} \left(u_z \frac{\partial}{\partial u_\perp} - u_\perp \frac{\partial}{\partial u_z} \right), \tag{A2}$$

$$\mathscr{E}_{n\alpha} = \mathscr{E}_{n\alpha}(k_\perp, \psi, \omega, z) \equiv E_r e^{i\psi} J_{n+1} + E_l e^{-i\psi} J_{n-1} \tag{A3}$$

J_n is the Bessel function of the order n and the argument $k_\perp u_\perp / \omega_{c\alpha}$. E_r and E_l are the circular polarized electric fields (5). ψ is the azimuth angle of $k_\perp$. It should be noticed that $k_z = k_z(k_\perp, \psi, \omega)$ is a complex value.

As can be seen immediately from Eq. (A1) diffusion takes place only for particles with a velocity u_z near the resonant velocity

$$v_{z\,\mathrm{res}} = \frac{\omega - l\omega_{ce}}{k_{zR}}, \qquad l = 0, \pm 1, \pm 2, \ldots$$

which is in our case the Alfvén velocity ($l=0$). The expression (A3) for the perpendicular E-field component reads with (5)

$$\mathscr{E}_{le} = \left[l \frac{\omega_{ce}}{k_x u_\perp} J_l + \frac{\omega^2}{2c^2} \frac{D}{k_x^2} (J_{l+1} - J_{l-1}) \right] E_x,$$

where $k_\perp \equiv k_x$ and S is neglected relative to P (4), (4a). For $l = 0$ this simplifies to

$$\mathscr{E}_{oe} = \frac{\omega^2}{2c^2} \frac{D}{k_x^2} \frac{u_\perp k_x}{\omega_{ce}} E_x + O\left[\left(\frac{u_\perp k_x}{\omega_{ce}} \right)^3 \right] \tag{A4}$$

The parallel E-field component has the form

$$J_o E_z = \frac{k_x k_{zR}}{k_x^2 + \frac{\omega_{ce}^2}{c^2}} E_x + O\left[\left(\frac{u_\perp k_x}{\omega_{ce}} \right)^2 \right] \tag{A5}$$

For regions in the magnetosphere, where the Alfvén velocity has its maximum, the argument of the Bessel function is less than 10^{-2} with k_x within the limits discussed. Since the ratio of the highest order terms of (A4) and (A5) is of the order of 1, Eq. (A1) now reads

$$\frac{\partial f'_{oe}}{\partial z} = \lim_{V\to\infty} \frac{1}{(2\pi)^3 V} \frac{e^2}{u_z m_e^2} \int_{-\infty}^{\infty} dk_x \, dk_y \, d\omega \cdot \left[|E_x|^2 \frac{k_x^2 k_{zR}^2}{\left(k_x^2 + \frac{\omega_{ce}^2}{c^2}\right)^2} \frac{\partial}{\partial u_z} \frac{i}{\omega - k_z u_z} \frac{\partial f'_{oe}}{\partial u_z} + O\left(\frac{u_\perp k_x}{\omega_{ce}} \right) \right]. \tag{A6}$$

Substituting (7) for $|E_x|^2$ and the dispersion relation

$$k_z^2 = S k_o^2 - \frac{S}{P} k_x^2.$$

for k_{zR}, the integration over ω has the form

$$\int_{-\infty}^{\infty} \omega \frac{\sin^2 \frac{T}{2}(\omega - \omega')}{(\omega - \omega')^2} d\omega = \pi \omega' \frac{T}{2}$$

noting, that k_{zI} is a linear function of ω. Since $k_x \ll \omega_{ce}/c$ the integration over k_x yields

$$\int_{-\infty}^{\infty} k_x^2 e^{-\frac{d^2 k_x^2}{8}} dk_x = \frac{8\sqrt{2\pi}}{d^3}.$$

Finally the diffusion equation becomes

$$\frac{\partial f'_{oe}}{dz} = \lim_{L_x \to \infty} \frac{\sqrt{2\pi}}{L_x d} \frac{E_0^2}{\mu_0} \frac{\omega'^2}{n_e m_e} \frac{S}{\omega_{pe}^2} \frac{1}{u_z} \frac{\partial}{\partial u_z} \frac{-k_{zI} u_z}{(\omega' - k'_{zR} u_z)^2 + (k_{zI} u_z)^2} \frac{\partial f'_{oe}}{\partial u_z} \tag{A7}$$

where the condition was used that all physical quantities must be real, which means $k_z(\omega) = -k_z^*(-\omega)$. Since the electron beam is spatially confined in the x-direction to the extent of the wave perpendicular to the ambient magnetic field, $L_x \approx d$ was taken. This leads to Equation (8).

References

Chiu, Y T., Schulz, M.: Self-consistent particle and parallel electrostatic field distributions in the magnetospheric-ionospheric auroral region. J. Geophys. Res. **83**, 629–642, 1978

Cornwall, J.M.: Micropulsations and the outer radiation zone. J. Geophys. Res. **71**, 2185–2199, 1966

Coronti, F.V., Kennel, C.F.: Electron precipitation pulsations. J. Geophys. Res. **75**, 1279–1289, 1970

Engel, R.D.: Nonlinear stability of the extraordinary wave in a plasma. Phys. Fluids **8**, 939–950, 1965

Fejer, J.A., Kan, J.R.: A guiding center Vlasov equation and its application to Alfvén waves. J. Plasma Phys. **3**, 331–351, 1969

Fejer, J.A., Lee, K.F.: Guided propagation of Alfvén waves in the magnetosphere. J. Plasma Phys. **1**, 387–406, 1967

Gendrin, R.. Pitch angle diffusion of low energy protons due to gyroresonant interaction with hydromagnetic waves. J. Atmos. Terr. Phys. **30**, 1313–1330, 1968

Gendrin, R.: General relationship between wave amplification and particle diffusion in a magnetoplasma. Rev. Geophys. Space Phys. **19**, 171–184, 1981

Hasegawa, A.. Kinetic properties of Alfvén waves. Proc. Indian Acad. Sci. **86**, 151–174, 1977

Kangas, J., Pikkarainen, T., Golikov, Yu., Baransky, L., Troitskaya, V.A., Sterlikova, V.: Bursts of irregular magnetic pulsations during the substorm. J. Geophys. **46**, 237–247, 1979

Kennel, C.F., Engelmann, F.: Velocity space diffusion from weak plasma turbulence in a magnetic field. Phys. Fluids **9**, 2377–2388, 1966

Kennel, C.F., Petschek, H.E.: Limit on stable trapped particle fluxes. J. Geophys. Res. **71**, 1–28, 1966

Kintner, P.M., Cahill, Jr., L.J.: Electric field oscillations measured near an auroral arc. Planet. Space Sci. **26**, 555–558, 1978

Klöcker, N., Theile, B.. Magnetic ULF-waves in the vicinity of active auroral forms. J. Geophys. **46**, 229–236, 1979

Mozer, F.S., Fahleson, U.V.. Parallel and perpendicular electric fields in an aurora. Planet. Space Sci. **18**, 1563–1571, 1970

Perraut, S., Gendrin, R., Robert, P., Roux, A., DeVilledary, C.. ULF-waves observed with magnetic and electric sensors on GEOS-1. Space Sci. Rev. **22**, 347–369, 1978

Petelski, E.F., Fahleson, U., Shawhan, S.D.: Models for quasi-periodic electric fields and associated electron precipitation in the auroral zone. J. Geophys. Res. **83**, 2489–2498, 1978

Stüdemann, W., Goertz, C.K.. Simultaneous observation of an intense 65 keV field-aligned proton beam and ULF-waves during a break-up event. J. Geophys. **49**, 123–127, 1981

Swift, D.W.. Mechanisms for the discrete aurora – A review. Space Sci. Rev. **22**, 35–75, 1978

S-300 Experimenters: Measurements of electric and magnetic wave fields and of cold plasma parameters onboard GEOS-1. Preliminary results. Planet. Space Sci. **27**, 317–339, 1979

Wilhelm, K., Klöcker, N., Theile, B., Ott, W., Spenner, K., Grabowski, R., Wolf, H., Stüdemann, W., Dehmel, G., Fischer, H.M., Schmidtke, G.L., Baumjohann, W., Pedersen, A., Jones, D., Riedler, W., Urban, A.: Observations of field-aligned current sheets above discrete auroral arcs. J. Geophys. **49**, 128–137, 1981

Received March 22, 1982; Revised version June 14, 1982
Accepted July 1, 1982